Acoustic Wave Scattering From a Rough Seabed Over a Sediment Layer With Generalized-Exponential Density and Inverse-Square Sound Speed Profiles

Jin-Yuan Liu, Sheng-Hsiung Tsai, Chung-Ray Chu, Yung-Hong Wu, and I-Chun Lin
Institute of Undersea Technology
National Sun Yat-sen University
Kaohsiung, 804 Taiwan
Email: jimliu@mail.nsysu.edu.tw

***Abstract*— This paper considers acoustic plane wave scattering from a rough seabed on a transition sediment layer overlying an elastic sea basement. The transition sediment layer is assumed to be fluid-like, with density and sound speed distributions behaving as generalized-exponential and inverse-square functions, respectively. This specific class of density and sound speed profiles deserves special attentions not only because it is geologically realistic, but also renders analytical solutions to the Helmholtz equation, making it particularly useful in the study of ocean and seabed acoustics. Based upon a boundary perturbation approach, the computational algorithm for the spatial spectrum in terms of the power spectral density of the scattered field has been developed and implemented. The results have shown that, while the coherent field mainly depends upon the gross structure of the seabed roughness, e.g., RMS roughness, the scattered field is significantly affected by the details of the roughness distributions specialized by the roughness power spectrum and the spatial correlation length of the rough surface. The dependence of the power spectral density of the scattered field on the various types of sediment stratifications, including the constant and the k^2-linear sound speed distributions, is also included in the analysis.**

I. Introduction

This paper concerns the problem of acoustic plane wave scattering from a rough seabed over a fluid-like sediment layer posessing a realistic class of density and sound speed distributions. The overall environmental model of this analysis is schematically shown in Figure 1, in which it illustrates an acoustic plane wave impinging upon a rough seabed with a non-uniform sediment layer overlying an elastic basement. The model includes three fundamental features of the seafloor environment: i) the seabed roughness, ii) the sediment non-uniformity, and iii) the basement shear property, and thus constitutes a canonical model in the study of ocean and seabed acoustics.

The specific classes of the density $\rho(z)$ and sound-speed $c(z)$ for the sediment layer to be considered here may be, respectively, described by:

$$\rho(z) = \frac{Ae^{\alpha z}}{\left(e^{\alpha z}+a\right)^2} \tag{1}$$

and

$$c(z) = \left[\frac{b^2}{\breve{c}_0^2} + \left(\frac{1}{\breve{c}_1^2} - \frac{b^2}{\breve{c}_0^2}\right)\frac{1}{(1-\kappa z)^2}\right]^{-1/2} \tag{2}$$

where A, α, a, $\breve{c}_1$, δ, b, $\breve{c}_0$, and κ are constant parameters. Equations (1) and (2) are respectively referred to as the generalized exponential density and the inverse-square sound speed profiles; a few examples of such profiles are shown in Figure 2. It has been demonstrated that, with a suitable choice of the parameters, this family of curves may well fit the experimental geoacoustic data [1]–[3]. Moreover, such density and sound speed combinations warrant special attentions not only because they are capable of describing a realistic seafloor environment, but also of providing analytical solutions for the acoustic wave equation (or Helmholtz equation), making them particularly valuable in the geoacoustic modeling.

The main theme of this paper is to consider the spatial energy distribution of the plane-wave scattered field, in terms of the power spectral density (PSD), for the environmental model described above. Along this line of research, the authors had previously analyzed another version of this problem in Ref. [4], in which the sound speed variations were treated to be either constant or k^2-linear (varying concave upward; cf. Figure 3), and no basement elasticity was considered.

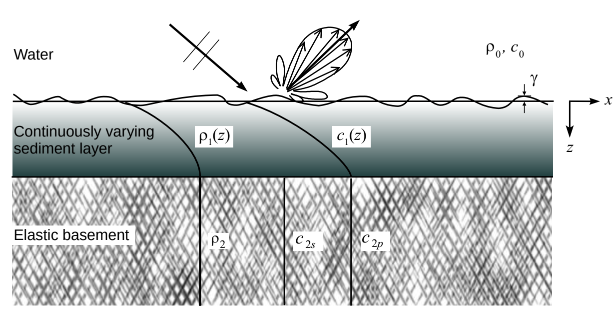

Fig. 1. A plane wave incident upon a rough seabed with a fluid-like sediment layer, subject to continuous variations in density and sound speed, overlying a uniform elastic basement.

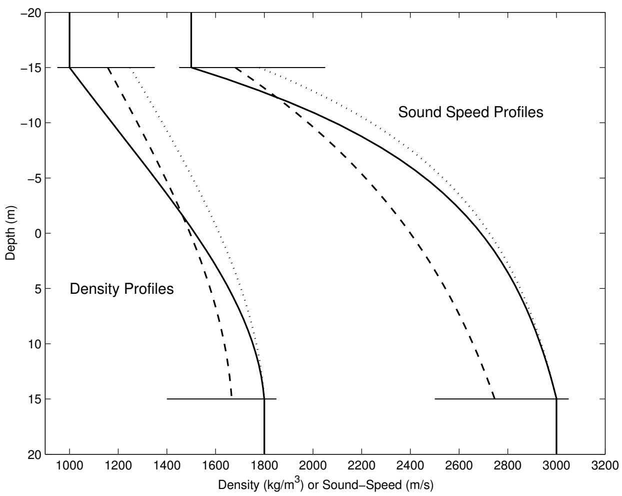

Fig. 2. Sample profiles for the generalized-exponential density and the inverse-square sound speed distributions for the functions shown in Equations (1) and (2).

For those cases, the solutions for the Helmholtz equation were either the expoenetial or the Airy's functions, and are readily implemented using current software, such as *Matlab*. In constrast, the present case of the inverse-square sound speed profile would lead to less tractable highly oscillatory Hankel functions of imaginary order, thus requiring special treament in the numerical implemetation. For this instance, the authors have found that a hybrid algorithm in conjunction with *Mathematica* [5] is particularly useful in this study.

In the analysis of wave scattering from rough surfaces, it customerily divides the total field into a coherent mean field and a random scattered field. The derivation process would generally arrive at an algorithm that the scattered field is driven by the mean field, and as a result, the coherent mean field must first be obtained. In this regard, the authors have acquired the soultions of the coherent field, and the results are presented in Ref. [6]. It has been found that the coherent reflection coefficients are very much dependent upon the type of variations in the sediment layer, in particular, a small difference between the k^2-linear and the inverse-square sound speed profiles may yield noticeably different results. Here, the emphases are placed on the energy distributions of the scattered field, as well as to identify the parameters that govern the distribution of scattering energy. It might be expected that, while the coherent field is only affected by the parameters describing the gross structure of the seabed roughness and the sediment stratification [6], the scattered field should depend upon both the gross and the fine structures of the sea-floor properties in a more sensitive manner; these are the subjects to be pursued in this paper.

In the following sections, we first summarize the relavant theories and develop the formulations for the problem at hand, then followed by numerical implementations and physical interpretations for a few representative examples.

II. **Formulations**

In this section, we describe the formulation for the power spectral density of the scattered field due to an acoustic plane wave impinging upon a rough surface over a horizontally-stratified medium. The formulations to be presented here are based upon the theory developed by Kuperman and Schmidt [7]–[9], in which both the mean (or coherent) and the scattered (incoherent) fields may be succinctly expressed by a few boundary operators in relation to the corresponding unperturbed (flat interface) problem. Therefore, we shall first present the solutions for acoustic wave propagation in a homogeneous medium, then continue to develop the formulation for acoustic wave scattering from rough surfaces. The presentation is intended to be brief and directly relevant to the present analysis, leaving the details of derivation for those interested readers to the original or previous articles [6], [9], [10], [11].

A. Acoustic wave propagation in a horizontally-stratified medium

Consider a two-dimensional monotonic acoustic plane wave of frequency ω, with time dependence of $e^{-i\omega t}$, propagating with a horizontal wavenumber k_x in a horizontally-stratified seismo-acoustic medium, such as one shown in Figure 1. The acoustic wave in layer j may generally be represented by [4]:

$$\chi_j(x,z) = \left[A_j^+(k_x)\mathcal{G}_j(k_x,z) + A_j^-(k_x)\mathcal{H}_j(k_x,z)\right] e^{ik_x x} \tag{3}$$

where χ_j is the acoustic variable, which for convenience is taken to be the acoustic pressure for a fluid layer, and the compressional or shear wave displacement potential for an elastic layer. The functions $\mathcal{G}_j$ and $\mathcal{H}_j$ represent the dependence of the acoustic wave on depth coordinate for each k_x, which for general stratification of density $\rho_j(z)$ and sound speed $c_j(z)$ may only be obtained through numerical procedure to the depth-dependent wave equation. Here, our interests lie on the specific cases for which the density and sound speed variations not only offer physically realistic model for the seafloor environment, but also provide analytical expressions for $\mathcal{G}_j$ and $\mathcal{H}_j$; further discussion shall be addressed later.

The unknown constants A_j^- and A_j^+ in Equation (3) are the amplitudes of the plane waves, which are determined by the physical constraints on the interfaces separating the layers. The conditions and the number of the physical constraints depend upon the types of boundary separating the media, e.g, a boundary separating a fluid and an elastic media requires continuities of the vertical displacement and the normal stress on the boundary, and moreover, the shear stress in the elastic medium must vanish. Application of boundary conditions results in a linear system, which may be conveniently expressed as:

$$\tilde{\mathcal{B}}(k_x)\tilde{\chi}(k_x) = \tilde{\mathcal{C}}(k_x) \tag{4}$$

where $\tilde{\mathcal{B}}(k_x)$ is a matrix containing the coefficients in the linear system, and $\tilde{\chi}(k_x)$ is a vector with the unknown constants $A_j^{\pm}(k_x)$ as its components, and $\tilde{\mathcal{C}}$ is a vector containing given source terms. By incorporating the radiation conditions, Equation (4) may be solved for the unknown amplitudes, and the solutions for the acoustic waves in each layer are then followed.

B. Acoustic plane wave scattering from rough surfaces and power spectral density

Based upon the solutions for the unperturbed flat interface problem described above, the formulation for acoustic wave scattering from rough surfaces may be derived. First, the total random field is decomposed into a mean (coherent) field $\langle\tilde{\chi}\rangle$ and a scattered (incoherent) field $\tilde{s}$:

$$\tilde{\chi} = \langle\tilde{\chi}\rangle + \tilde{s} \tag{5}$$

where $\tilde{s}$ is a random variable, and is the same order of magnitude as the surface roughness γ, which is assumed to be small in comparison with the acoustic wavelength and the layer thickness. Then, a procedure of small-parameter perturbation is employed on the boundary conditions, referred to as boundary perturbation method, to derive the formulations for the mean and the scattered fields.

The derivation using boundary perturbation method leads to the following modified linear system for the mean field [9]:

$$\left[\tilde{\mathcal{B}}(k_x) + \frac{\langle\gamma^2\rangle}{2}\frac{\partial^2}{\partial z^2}\tilde{\mathcal{B}}(k_x) + \tilde{I}(k_x)\right]\langle\tilde{\chi}(k_x)\rangle = \tilde{\mathcal{C}}(k_x) \tag{6}$$

where $\langle\gamma^2\rangle$ is the mean-squared roughness, and $\tilde{I}$ is a scattering operator given by:

$$\begin{aligned}\tilde{I}(k_x) &= -\frac{\langle\gamma^2\rangle}{\sqrt{2\pi}}\int dq_x P_b(q_x - k_x)\\ &\quad\times\left[\frac{\partial}{\partial z}\tilde{\mathcal{B}}(q_x) - i(k_x - q_x)\circ\tilde{b}(q_x)\right]\\ &\quad\times\tilde{\mathcal{B}}^{-1}(q_x)\left[\frac{\partial}{\partial z}\tilde{\mathcal{B}}(k_x) - i(q_x - k_x)\circ\tilde{b}(k_x)\right]\end{aligned} \tag{7}$$

where P_b is the power spectrum of the rough surface, and $\tilde{b}$ is a matrix representing the effects of rough-surface orientation in terms of unperturbed problem; the operation $\circ$ is either the inner or the outer product, depending upon the types of boundary conditions.

Once the mean field is determined from Equation (6), the scattered field due to an incident plane wave with horizontal wavenumber k_x may be obtained according to the following formulation:

$$\begin{aligned}\tilde{s}(q_x) &= -\frac{1}{2\pi}\tilde{\gamma}(q_x - k_x)\tilde{\mathcal{B}}^{-1}(q_x)\\ &\quad\times\left[\frac{\partial}{\partial z}\tilde{\mathcal{B}}(k_x) - i(q_x - k_x)\circ\tilde{b}(k_x)\right]\langle\tilde{\chi}(k_x)\rangle\end{aligned} \tag{8}$$

where $\tilde{\gamma}$ is the Fourier spectrum of the surface roughness. The formulation clearly indicates that the scattered field is driven by the coherent field. It then may be shown that the expectation value of the power spectral density, $\langle\tilde{s}(q_x)\tilde{s}^*(q_x)\rangle$, of the scattered field is [9]:

$$\begin{aligned}\langle\tilde{s}(q_x)\tilde{s}^*(q_x)\rangle &= \frac{\langle\gamma^2\rangle}{2\pi}P_b(q_x - k_x)\\ &\quad\times\Bigg|\tilde{\mathcal{B}}^{-1}(q_x)\left[\frac{\partial}{\partial z}\tilde{\mathcal{B}}(k_x)\right.\\ &\quad\left.-i(q_x - k_x)\circ\tilde{b}(k_x)\right]\langle\tilde{\chi}(k_x)\rangle\Bigg|^2\end{aligned} \tag{9}$$

The above formulation describes the wavenumber or angular distribution of the scattered energy, and is the formulus to be employed in the later analysis.

C. Relevant operators

Here we present the relevant operators, $\tilde{\mathcal{B}}$, its derivatives, and $\tilde{b}$, shown in Equation (9), for the problem depicted in Figure 1. Since these operators only involve the solutions for the corresponding unperturbed problem, the solutions for the Helmholtz equation in each layer must first be derived.

As discussed previously, for an incident plane wave with horizontal wavenumber k_x, the solutions of the Helmholtz equation may be expressed as a form of Equation (3), which when written explicitly for each individual layer in the present problem are as follows:

$$p_0(x,z) = A_0^-(k_x)e^{-ik_{0,z}z}e^{ik_x x} \tag{10}$$

$$\begin{aligned}p_1(x,z) &= \left[A_1^+(k_x)\mathcal{G}(k_x,z) + A_1^-(k_x)\mathcal{H}(k_x,z)\right]\\ &\quad\times e^{ik_x x}\end{aligned} \tag{11}$$

$$\phi_2(x,z) = A_2^+(k_x)e^{ik_{2p,z}z}e^{ik_x x} \tag{12}$$

$$\psi_2(x,z) = B_2^+(k_x)e^{ik_{2s,z}z}e^{ik_x x} \tag{13}$$

where $\mathcal{G}(k_x,z)$ and $\mathcal{H}(k_x,z)$ are the solutions of the depth-dependent wave equation in the sediment layer, and the vertical wavenumber $k_{j,z}$ in various layers are given as follows:

$$k_{0,z}^2 = k_0^2 - k_x^2 \tag{14}$$

$$k_{2p,z}^2 = k_{2p}^2 - k_x^2 \tag{15}$$

$$k_{2s,z}^2 = k_{2s}^2 - k_x^2 \tag{16}$$

where $k_0 = \omega/c_0$, $k_{2p} = \omega/c_{2p}$, and $k_{2s} = \omega/c_{2s}$ are the medium wavenumbers.

For the sediment layer, although our primary interest of this paper lies on the solutions for the density and sound speed profiles stipulated by Equation (1) and (2), however, for comparison purpose, both the cases of constant and k^2-linear sound speed profiles shall be included in later discussion. Thus, the sound speed distributions are:

$$\frac{1}{c^2(z)} = \begin{cases}\frac{1}{\tilde{c}_1^2}, & \text{constant}\\ \frac{(1+\delta z)}{\tilde{c}_1^2}, & k^2\text{-linear}\\ \frac{b^2}{\tilde{c}_0^2} + \left(\frac{1}{\tilde{c}_1^2} - \frac{b^2}{\tilde{c}_0^2}\right)\frac{1}{(1-\kappa z)^2}, & \text{inverse-square}\end{cases} \tag{17}$$

It has been shown that the exact solutions for the Helmholtz equation exist if the density follows Equation (1), *and* the sound speed profiles satisfy one of the functions in Equation (17) [10], [14]–[16]; an example containing three different types of sound speed profiles is shown in Figure 3.

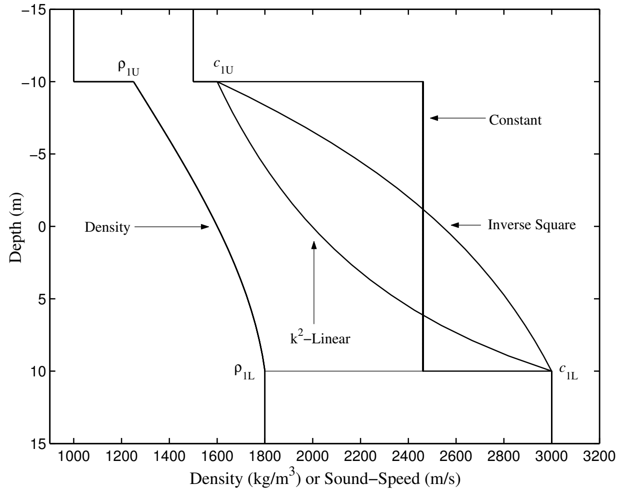

Fig. 3. Sample profiles for density and three types of sound speed distributions; values for various parameters are (units omitted): $A = 3553$, $\alpha = -0.0544$, $a = 0.490$, $\breve{c}_1 = 2461, 2351, 2542$ (for constant, k^2-linear, inverse-square sound speed profile, respectively), $\delta = -0.0557$, $b = 1.5$, $\breve{c}_0 = 5434$, and κ=-0.05. For comparison purpose, the constant sound $\breve{c}_1$ is taken to be the geometric mean of the inverse-square profile.

The solutions for the sediment layer corresponding to various profiles described above may be expressed as:

$$p_1(x,z) = \tilde{p}_1(z) e^{ik_x x} \tag{18}$$

with the depth dependence of the pressure field given by [10]–[13]:

$$\tilde{p}_1(z) = \sqrt{\rho(z)} \begin{cases} e^{i\sigma z}, \ e^{-i\sigma z} \\ \mathrm{Ai}(\eta(z)), \ \mathrm{Bi}(\eta(z)) \\ \sqrt{\zeta(z)} H_\nu^{(1)}(\beta\zeta(z)), \ \sqrt{\zeta(z)} H_\nu^{(2)}(\beta\zeta(z)) \end{cases} \tag{19}$$

where the first, second, and third rows on the right-hand-side of the above equation correspond to the solutions for the constant, k^2-linear, and inverse-square sound-speed profiles, respectively, and Ai, Bi are the Airy functions, and $H_\nu^{(1)}$, $H_\nu^{(2)}$ are the νth-order Hankel functions; relevant parameters/variables are defined below:

$$\sigma^2 = \frac{\alpha^2}{4} - \breve{k}_1^2 \sin^2\theta_1 \tag{20}$$

$$\eta(z) = -\frac{1}{\sqrt[3]{\left(\breve{k}_1^2\delta\right)^2}} \times \left(\breve{k}_1^2 \delta z + \breve{k}_1^2 - \breve{k}_0^2 \cos^2\theta_0 - \frac{\alpha^2}{4}\right) \tag{21}$$

$$\zeta(z) = 1 - \kappa z \tag{22}$$

$$\beta^2 = \frac{1}{\kappa^2}\left(\breve{k}_0^2 b^2 - \breve{k}_0^2\cos^2\theta_0 - \frac{\alpha^2}{4}\right) \tag{23}$$

$$\nu^2 = \frac{1}{4} - \frac{\omega^2}{\kappa^2}\left(\frac{1}{\breve{c}_1^2} - \frac{b^2}{\breve{c}_0^2}\right) \tag{24}$$

with $\breve{k}_1 = \omega/\breve{c}_1$ and θ_1 defined as $\breve{k}_1\cos\theta_1 = \breve{k}_0\cos\theta_0$. Therefore, the functions $\mathcal{G}$ and $\mathcal{H}$ in Equation (11) are one of the solution sets in Equation (19), depending upon the sediment profiles.

It is noticed from Equation (24) that for high frequency, or any other factor rendering ν^2 negative, the Hankel function becomes imaginary orders. As mentioned previously, while both the Airy functions and the Hankel functions are generally built-in in most computational software, the imaginary order of Hankel functions may not be readily available, so that a special treatment is generally needed [10].

With the solutions for the unperturbed problem now available, the relevant operators are readily derived. For the unknown vector $\tilde{\chi}(k_x)$ defined as:

$$\tilde{\chi}(k_x) = \left[A_0^-(k_x) \ A_1^+(k_x) \ A_1^-(k_x) \ A_2^+(k_x) \ B_2^+(k_x)\right]^T \tag{25}$$

the coefficient matrix $\tilde{\mathcal{B}}(k_x)$ and the source vector $\tilde{\mathcal{C}}(k_x)$ in Equation (4) are, respectively, given by:

$$\tilde{\mathcal{B}}(k_x) = \begin{bmatrix} 1 & -\mathcal{G}(k_x,-h/2) & -\mathcal{H}(k_x,-h/2) & 0 & 0 \\ \frac{ik_{0,z}}{\rho_1\omega^2} & \frac{1}{\rho_{1U}\omega^2}\mathcal{H}'(k_x,-h/2) & \frac{1}{\rho_{1U}\omega^2}\mathcal{G}'(k_x,-h/2) & 0 & 0 \\ 0 & \mathcal{G}(k_x,h/2) & \mathcal{H}(k_x,h/2) & \mu\left(2k_x^2 - k_{2s,z}^2\right) & \mu 2k_x k_{2s,z}^2 \\ 0 & \frac{1}{\rho_{1L}\omega^2}\mathcal{G}'(k_x,h/2) & \frac{1}{\rho_{1L}\omega^2}\mathcal{H}'(k_x,h/2) & -ik_{2p,z} & ik_x \\ 0 & 0 & 0 & -2k_x k_{2p,z} & k_x^2 - k_{2s,z}^2 \end{bmatrix} \tag{26}$$

$$\tilde{\mathcal{C}}(k_x) = S_\omega \begin{bmatrix} -\frac{1}{i4\pi k_{0,z}} & \frac{1}{\rho_1\omega^2 4\pi} & 0 & 0 & 0 \end{bmatrix}^T \tag{27}$$

where ρ_{1U} (c_{1U}) and ρ_{1L} (c_{1U}) are, respectively, the density (sound speed) at the upper and the lower boundary of the sediment layer; the superscript $'$ is the derivative with respect to z. Moreover, the rotational matrix $\tilde{b}$ is:

$$\tilde{b}(k_x) = \begin{bmatrix} \frac{-ik_x}{\rho_1\omega^2} & \frac{ik_x}{\rho_{2U}\omega^2}\mathcal{G}(k_x,-h/2) & \frac{ik_x}{\rho_{2U}\omega^2}\mathcal{H}(k_x,-h/2) & 0 & 0 \\ 0 & 0 & 0 & 0 & 0 \\ 0 & 0 & 0 & 0 & 0 \\ 0 & 0 & 0 & 0 & 0 \\ 0 & 0 & 0 & 0 & 0 \end{bmatrix} \tag{28}$$

III. **Results and discussion**

Equation (9), along with the related formulations and operators, may now be numerically implemented to compute the spatial power spectral density of the scattered field. Since there are numerous variables and parameters in the problem, some

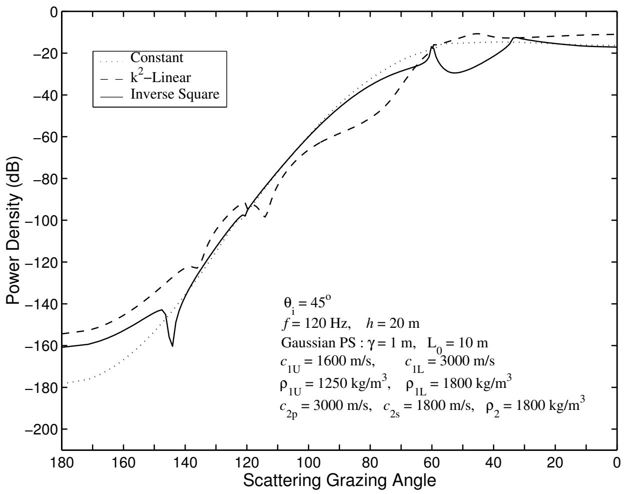

Fig. 4. Scattering power spectral density for rough seabed with Gaussian roughness power spectrum, and for the environmental model shown in Figure 3, at incident angle of 45° and frequency of 120 Hz.

Fig. 5. Gaussian roughness power levels as function of scattering wavenumber for frequency of 100, 110, and 120 Hz; incoming wave incident at 45°.

of them are taken to be constant values, e.g., $c_0 = 1500$ m/s, $\rho_0 = 1000$ kg/m^3, For the seabed roughness, either the Gaussian spectrum or the Goff-Jordan power-law spectrum [17] is employed; these spectra are defined as follows:

$$P_b(k_x) = \begin{cases} \sqrt{2\pi} L_0 \exp\left(\frac{k_x^2 L_0^2}{2}\right), & \text{Gaussian} \\ \frac{4k_*^3}{(k_x^2+k_*^2)^2}, & \text{Goff-Jordan} \end{cases} \tag{29}$$

where L_0 is the correlation length, and k_* represents a characteristic wavenumber of the rough surface.

Figure 4 shows the power spectral density for a 120 Hz plane wave incident at 45° upon a rough seabed with Gaussian roughness spectrum; the density and sound speed profiles in the sediment layer are shown in Figure 3. It is first noted that the spatial domain with grazing angle lower/higher than 90° is within the forward/backward scattering sector. The solid, dashed, and dotted curves are, respectively, the spatial spectra for the inverse-square, k^2-linear, and constant sound speed profiles in the sediment. The results have shown that more energy is scattered into the forward sector than into the backward section, which basically is governed by the Bragg's law of scattering in that the scattering power density is weighted by the "translated" roughness power spectrum $P_b(q_x - k_x)$, which is shown in Figure 5 for an incoming wave with incident angle of 45°. The roughness power levels reach maxima at scattering wavenumbers ($q_x = k\cos\theta_0$) of about 0.296, 0.326, 0.355 m^{-1}, respectively, for 100, 110, and 120 Hz. In terms of scattering angles in real space (between 0° and 180°), the power spectra increase from the backward towards the forward sector (from 180° to 0°), and attain maxima at scattering angle of 45°, as shown in Figure 6.

Fig. 6. Gaussian roughness power levels as function of scattering wavenumber for frequency of 100, 110, and 120 Hz; incoming wave incident at 45°.

Each of the three curves in Figure 4 demonstrates a special feature in its variation: for example, the dotted curve (constant profile) increases smoothly from 180° to 0° (backward to forward sector), while the other two curves have a few "peaks/notches". The smoothness of the dotted curve and the similarity between this curve and the roughness power spectra shown in Figure 6 signify that the seabed roughness on the water-sediment interface is the dominant factor for the scattering energy distribution; the sediment-basement interface plays an insignificant role in this case. In other words, the strong contrast between the water-sediment interface reflects and scatters most of the incoming energy, leaving only little energy across the upper boundary to interact with the sediment-basement interface.

On the other hand, the inverse-square sound speed profile is of a relatively mild variation, so that the incoming and the scattered waves may penetrate into the sediment layer and interact with lower interface. This is indicated by the noticeable spikes at $\cos^{-1}(1500/3000) = 60^\circ$ and 120° and those at $\cos^{-1}(1500/1800) \simeq 34^\circ$ and 146°, which correspond to the critical angles of the compressional and shear waves in the basement, respectively. As for the case of k^2-linear profile, the scattering spectrum (dashed curve) demonstrates a similar variation as that for inverse-square case, except that the "peaks/notches" are displaced due to varied stratification.

The result for the same scenario as in Figure 4 but for frequency of 100 Hz is shown in Figure 7. A comparison of these two figures illustrates that, as the frequency decreases, more and more energy is scattered into the backward sector. This is easily understood in view of Figure 6, in that the seabed roughness possesses higher power density for lower frequency, particularly for lower grazing angles in the backward sector.

In what follows, the effects of various parameters/variables on the scattering power spectral density are examined. Since the inverse-square profile is the primary concerns of this paper, furthermore, the results for this profile are still very limited in literature, therefore, unless otherwise mentioned, the inverse-square profile as shown in Figure 2 is employed in the following analysis.

Figure 8 presents the power spectral density corresponding to the environment shown in Figure 3 for three values of frequency. It shows that the power spectral density is higher for higher frequencies, particularly in the backward sector. This is compatible with the variation of roughness power spectra shown in Figure 6. Physically, as the frequency becomes lower, the incident wave mainly confronts (or resonates) with the larger-scale roughness, which contains higher power within the roughness spectrum; as a result, the scattering power density becomes higher.

Figure 9 illustrates the scattering power spectral density for

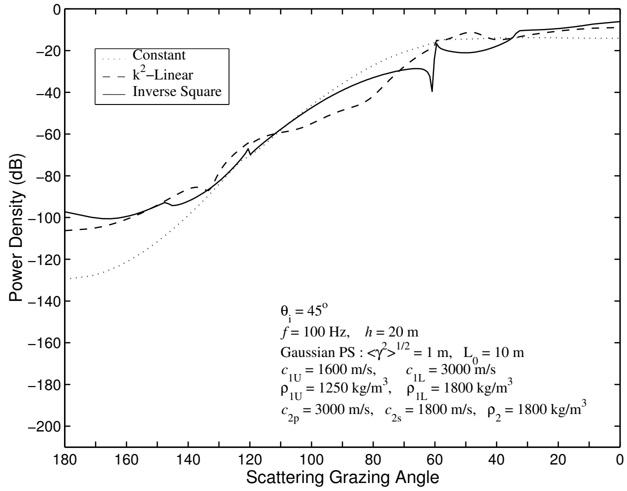

Fig. 7. Scattering power spectral density for rough seabed with Gaussian roughness power spectrum, and for the environmental model shown in Figure 3, at incident angle of 45° and frequency of 100 Hz.

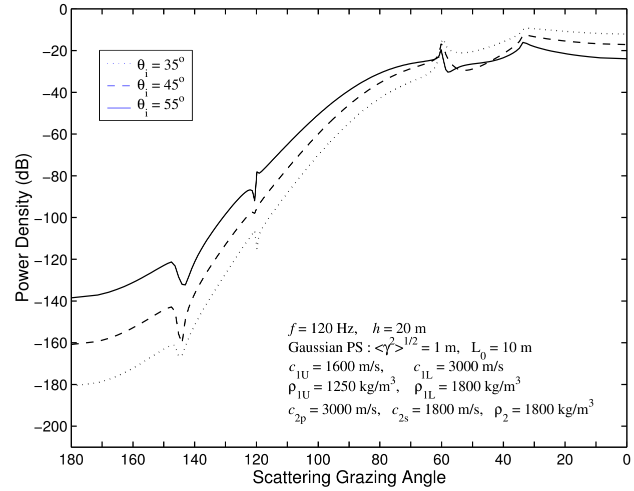

Fig. 9. Scattering power spectral density for various incident angle, and for Gaussian roughness seabed on a sediment layer with an inverse-square profile, at frequency of 120 Hz.

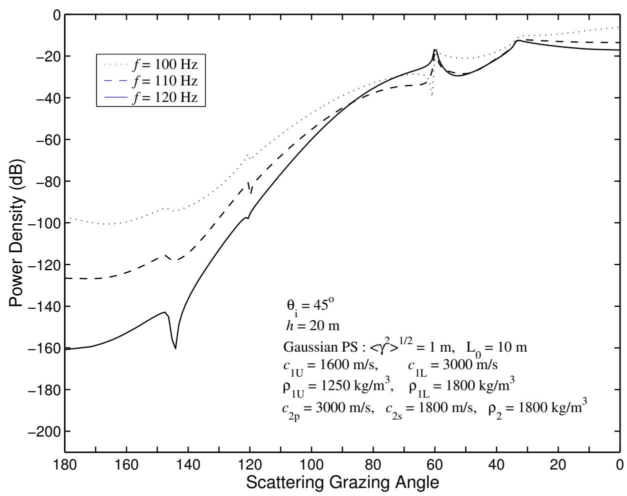

Fig. 8. Scattering power spectral density for various frequencies, and for Gaussian roughness seabed on a sediment layer with an inverse-square profile, at incident angle of 45°.

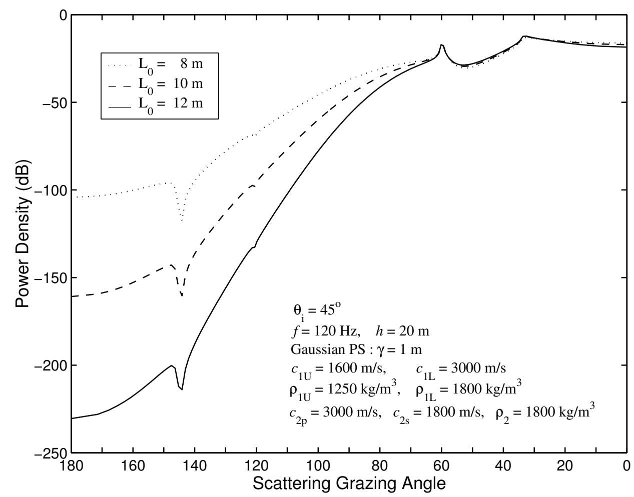

Fig. 10. Spatial power spectral density for Gaussian roughness power spectrum with various correlation lengths, at incident angle 45° and frequency 120 Hz, and for inverse-square sound speed profile in the sediment layer.

various incident angles. It shows that, when the incident grazing angle becomes shallower, more and more energy is shifted from the backward to the forward sector, with a “turning point” at about 60° in this case (to be discussed below, cf. Figure 11). This is consistent with the general principle stipulating that a shallow-angle incident wave produces more forward scattering energy.

Figure 10 presents the scattering power spectral density for various correlation lengths in the Gaussian roughness spectrum. It is noted that, when the correlation length changes, the power spectral density changes significantly, particularly in the backward sector. Physically, a power spectrum with a smaller correlation length represents a rough surface containing more energy in the higher wavenumber components, or equivalently, a rougher surface. Therefore, the incident wave faces a rough surface with a more randomized distribution, resulting in a stronger backward scattering. It is also noticed that for the scattering grazing angles lower than about 60° in the forward sector, the scattering spectral density is little affected by the correlation length. This should be compared with Figure 11, in which the “translated” Gaussian power levels for the three correlation lengths are shown. It is seen that the three curves have large differences for lower grazing angles in the backward sector, increasing levels towards forward sector, and then converging at near 60°. Therefore, the distributions of both Figures 9 and 10 are in effect dominated by the roughness power spectrum.

The effects of RMS roughness on the power spectral density is shown in Figure 12. Here, the power spectral densities for RMS roughness of 0.3, 0.5, and 1 m in the Gaussian roughness

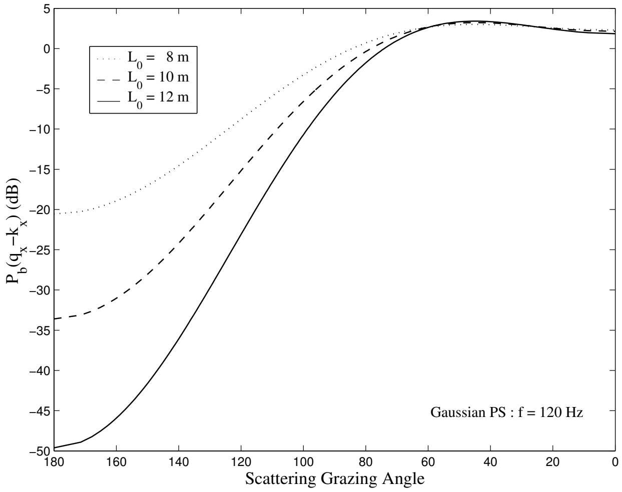

Fig. 11. "Translated" Gaussian roughness power levels as function of scattering wavenumber for correlation length of 8, 10, and 12 m; incoming wave incident at 45°.

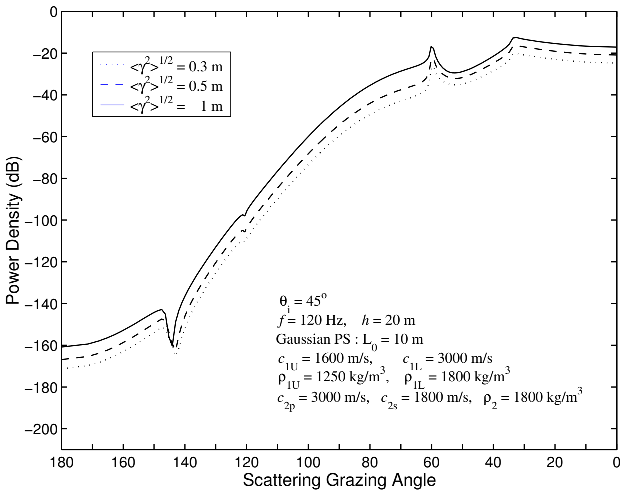

Fig. 12. Spatial power spectral density for various RMS roughness in Gaussian Roughness power spectrum, at incident angle of 45° and frequency of 120 Hz, and for inverse-square sound speed profile in sediment layer.

power spectrum are illustrated. The results have shown that the larger the RMS roughness, the higher the spectral density, indicating that an increase of RMS roughness is to enhance the rough surface scattering as expected.

Finally, the power spectral densities for the scattered field due to a rough surface describable by the Goff-Jordan roughness spectrum are shown in Figure 13; here, the results are for the environment shown in Figure 3. The distributions of the power spectral density in this case are in vast difference with those due to a rough surface with Gaussian spectrum shown in the previous figures; in particular, the backscattering is greatly enhanced. This is clearly due to the characteristics of the Goff-Jordan roughness power spectrum, shown in Figure 14 for three values of frequency, in which it demonstrates that the energy in the high-wavenumber components (or equivalently,

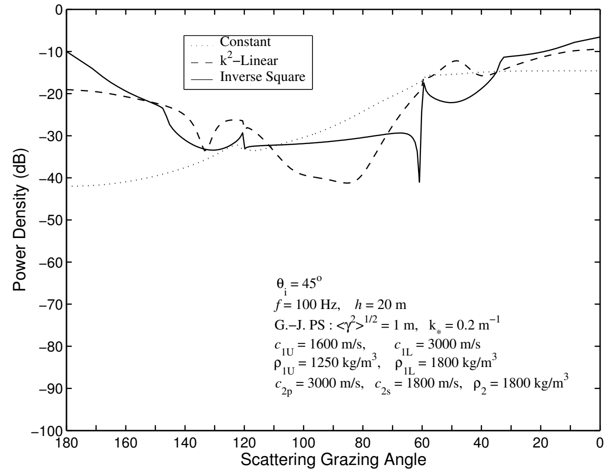

Fig. 13. Spatial power spectral density for Goff-Jordan roughness power spectrum, at incident angle of 45° and frequency of 100 Hz.

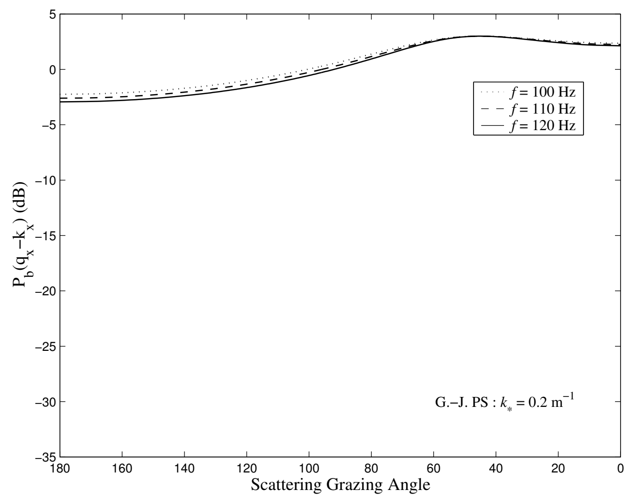

Fig. 14. "Translated" Goff-Jordan roughness power spectra, for incident angle of 45° and for frequency of 100, 110, and 120 Hz.

low grazing angles in the backward sector) is much higher in comparison with that for the Gaussian spectrum. Furthermore, the Goff-Jordan roughness spectrum is more evenly distributed throughout the scattering space, making the distributions of the power spectral density less difference between the forward and the backward sectors accordingly.

IV. Concluding Remarks

This paper investigates the spatial power spectral density of acoustic plane wave scattering from a rough seabed on a non-uniform sediment layer overlying an elastic basement. The emphasis of discussion is placed on the case in which the sediment layer possesses a density distribution as a generalized exponential function, and a sound speed as an inverse square function. This environmental model provides an appropriate simulation for an acoustic wave scattering from a realistic sea floor.

The results have indicated that, for low frequency (e.g., hundred Hertz or so), there are two factors affecting the distributions of the scattered energy: the seabed roughness and the sediment stratification, with the former being the dominating factor. Both the RMS roughness and the spatial correlation length of the seabed roughness have strong effects on the distributions of the power spectral density; furthermore, the type of roughness power spectrum employed also has significant effects in shaping the power spectral density of the scattered field. In addition, the variations of acoustic properties in the sediment affect the degree of penetration for the acoustic energy into the sea floor. All of these results clearly demonstrate the importance of correct use of a sea floor model in the study of acoustic scattering from a rough seabed.

ACKNOWLEDGMENTS

This work was supported in part by National Science Council of Taiwan, R.O.C. through contract NSC90-2611-E-110-009, and in part by the Ministry of Education of Taiwan, R.O.C. under the joint project between National Cheng-Kung University and National Sun Yat-sen University.

REFERENCES

[1] E.L. Hamilton, "Sound speed and related properties of sedments from experimental mohole (Guadalupe site)," *Geophysics*, vol. 30, pp. 257–261, 1965.

[2] E.L. Hamilton, "Sound velocity gradient in marine sediments," *J. Acoust. Soc. Am.*, vol. 65, pp. 909–922, 1979.

[3] E.L. Hamilton, "Geoacoustic modeling of the sea floor," *J. Acoust. Soc. Am.*, vol. 68, pp. 1313–1340, 1980.

[4] J.-Y. Liu and C.-F. Huang, "Acoustic plane-wave scattering from a rough interface over an inhomogeneous transition fluid layer," *Ocean Engineering*, vol. 28, no. 6, pp. 603-619, 2001.

[5] S. Wolfram, S., *The Mathematica Book*, 3rd edi., Cambridge University Press, 1996.

[6] J.-Y. Liu, C.-C. Wang, S.-H. Tsai, C.-R. Chu, "Acoustic wave reflection from a rough seabed with a continuously varying sediment layer overlying an elastic basement," *J. Sound and Vibration* (in press).

[7] H. Schmidt and W.A. Kuperman, "A full wave solution for propagation in multilayered viscoelastic media with application to gaussian beam reflection at fluid-solid interface," *J. Acoust. Soc. Am.*, vol. 77(3), pp. 831–825, 1985.

[8] W.A. Kuperman and H. Schmidt, "Rough surface elastic wave scattering in a horizontally stratified ocean," *J. Acoust. Soc. Am.*, vol. 79(6), pp. 1767–1777, 1986.

[9] W.A. Kuperman and H. Schmidt, "Self-consistent perturbation approach to rough surface scattering in stratified elastic media," *J. Acoust. Soc. Am.*, vol. 86, pp. 1511–1522, 1989.

[10] A.J. Robins, "Reflection of plane acoustic wave from a layer of varying density," *J. Acoust. Soc. Am.*, vol. 87(4), pp. 1546–1552, 1990.

[11] A.J. Robins, "Reflection of a plane wave from a fluid layer with continuously varying density and sound speed," *J. Acoust. Soc. Am.*, vol. 89(4), pp. 1686–1696, 1991.

[12] A.J. Robins, "Exact solutions of the Helmholtz equation for plane wave propagation in a medium with variable density and sound speed," *J. Acoust. Soc. Am.*, vol. 93(3), pp. 1347–1352, 1993.

[13] A.J. Robins, "Generation of shear and compression waves in an inhomogeneous elastic medium," *J. Acoust. Soc. Am.*, vol. 96(3), pp. 1669–1676, 1994.

[14] I. Tolstoy, "The theory of waves in stratified fluids including the effects of gravity and rotation," *Rev. Mod. Phys.*, vol. 35, pp. 207–230, 1963.

[15] I. Tolstoy, "Effects of density stratification on sound waves," *J. Geophys. Res.*, vol. 70(24), pp. 6009–6015, 1965.

[16] A.O. Williams and D.R. MacAyeal, "Acoustic reflection from a sea bottom with linearly increasing sound speed," *J. Acoust. Soc. Am.*, vol. 66, pp. 1836–1841, 1979.

[17] J.A. Goff and T. Jordan, "Stochastic modeling of seafloor morphology: Inversion of Sea Beam data for second-order statistics," *J. Geophys. Res.*, vol. 93, pp. 13589–13608, 1988.